# Finite volume approximation of a diffusion-dissolution model and application to nuclear waste storage

O. Angelini, C. Chavant, Eric Chénier, Robert Eymard, S. Granet

# Finite volume approximation of a diffusion-dissolution model and application to nuclear waste storage[1]

O. Angelini[a,b], C. Chavant[a], E. Chénier[b], R. Eymard[b], S. Granet[a]

[a] *Laboratoire de Mécanique des Structures Industrielles Durables, UMR EDF/CNRS 2832, France*
[b] *Université Paris-Est, 5 bd Descartes, 77454 Marne-la-Vallée, France*

**Abstract**

The study of two phase flow in porous media under high capillary pressures, in the case where one phase is incompressible and the other phase is gaseous, shows complex phenomena. We present in this paper a numerical approximation method, based on a two pressures formulation in the case where both phases are miscible, which is shown to also handle the limit case of immiscible phases. The space discretization is performed using a finite volume method, which can handle general grids. The efficiency of the formulation is shown on three numerical examples related to underground waste disposal situations.

*Keywords:*
Two phase Darcy flow in porous media; finite volume method; nuclear waste storage.

## 1. Introduction

A large community of scientists is concerned by understanding the mechanical and hydraulic behaviour of deep repository radioactive waste, in reason of its large impact on environment and human safety. This implies to be able to model and simulate complex phenomena such as the de-saturation and re-saturation of geological media, gas production induced by the corrosion of steel containers, within complex 3D heterogeneous and anisotropic domains including singular zones such as galleries and cells intersections. Moreover, materials with highly contrasted physical properties are involved in long time phenomena (from thousand to millions of years).

Hence the simulation of these physical features happens to be a complex task, and their validation is a major concern for the safety improvement of the industrial devices. Computational benchmarks, such as the Couplex Gaz benchmark [18], are useful for the definition of relevant physical models and numerical methods. Indeed, the Couplex Gaz benchmark has shown that the Darcy flow of two immiscible phases, the first one being an incompressible liquid phase and the second one the gaseous phase, can lead, in presence of high capillary pressures, to unphysical situations and to drastic numerical difficulties. This model implies the displacement of a free boundary between zones where the two fluid phases are simultaneously present (called in this paper the "under-saturated" zone) and zones where the only present fluid phase is the liquid phase (called in this paper the "saturated" zone). In an unexpected way, it can lead to the existence of zones where the liquid phase has been removed because of capillary forces and cannot be instantaneously replaced by the gaseous phase, hence creating a vacuum volume. It is interesting to exhibit the origin of such behaviour from the immiscible model equations, that we now describe. Throughout all this paper, we shall denote by $l$ and $g$ the liquid and gaseous phases, and by $w$ and $h$ the water and gas components (the choice of $h$ for the gas component is linked with the fact that this model should apply to hydrogen generation due to acid attack of metallic containers, which may arise during long term storage). In the immiscible model, the liquid phase only

*Email addresses:* ophelie-externe.angelini@edf.fr ( O. Angelini ), clement.chavant@edf.fr ( C. Chavant), eric.chenier@univ-mlv.fr ( E. Chénier), robert.eymard@univ-mlv.fr ( R. Eymard), sylvie.granet@edf.fr ( S. Granet)

contains the water component and the gaseous phase only contains the gas component. This leads to the following conservation equations:

$$\left\{\begin{array}{l} \dfrac{\partial(\phi(\mathbf{x})\rho_l S_l)}{\partial t} - \mathrm{div}\Big(\mathbf{k}(\mathbf{x})\dfrac{\rho_l k_{rl}(S_l)}{\mu_l}(\nabla P_l - \rho_l \mathbf{g})\Big) = 0, \\ \dfrac{\partial(\phi(\mathbf{x})\rho_g(P_g)(1-S_l))}{\partial t} - \mathrm{div}\Big(\mathbf{k}(\mathbf{x})\dfrac{\rho_g(P_g)k_{rg}(S_l)}{\mu_g}(\nabla P_g - \rho_g(P_g)\mathbf{g})\Big) = 0, \\ P_g - P_l = P_c(S_l) \text{ and } \rho_g(P_g) = M^h P_g/RT. \end{array}\right. \tag{1}$$

In (1), the density of the liquid phase $\rho_l$ is assumed to be constant, that of the gaseous phase $\rho_g(P_g)$ is given by the ideal gas law, the phase viscosities $\mu_l$ and $\mu_g$ are constant, the relative permeabilities $k_{rl}(S_l)$, $k_{rg}(S_l)$ and capillary pressure $P_c(S_l)$ functions are given for example by Van Genuchten laws. In the Couplex Gaz benchmark [18], some materials happen to have a very low permeability ( $\mathbf{k}(\mathbf{x})$ varies between $10^{-14}$ and $10^{-21}$ m$^2$) and the intensity of the capillary pressures is very high, about $10^7$ Pa. The porosity $\phi(\mathbf{x})$ varies within the range $[0.05, 0.3]$. A consequence of such data is that the initial gas pressure remains negligible (with an order of magnitude about $10^5$ Pa), compared to the liquid pressure, whose order of magnitude (which is negative, as it is classical for such high capillary pressures) is about $-10^7$ Pa. Hence, to a first approximation, $P_g - P_l \simeq -P_l$, and the liquid saturation can be approximately solved by the relation

$$S_l = C(-P_l),$$

where the capacity function $C(P)$ is, as in the case of Richards equation, the reciprocal function of the capillary pressure for $P \geq 0$ and equal to 1 for $P \leq 0$ (see Figure 1). Substituting this expression into the liquid component conservation equation, we get that $P_l$ is solution of the following equation, which appears to be (again, to a first approximation) decoupled from the gas conservation equation:

$$\frac{\partial(\phi(\mathbf{x})\rho_l C(-P_l))}{\partial t} - \mathrm{div}\Big(\mathbf{k}(\mathbf{x})\frac{\rho_l k_{rl}(C(-P_l))}{\mu_l}(\nabla P_l - \rho_l \mathbf{g})\Big) = 0. \tag{2}$$

Then Equation (2) is the classical Richards equation (which is of elliptic/parabolic type). The solution of this well-posed problem, denoted by $P_l(\mathbf{x}, t)$, allows for expressing the liquid saturation by $S_l(\mathbf{x}, t) = C(-P_l(\mathbf{x}, t))$. Let us now consider the gas conservation equation, divided by $M^h/RT$, in which we now assume that the liquid saturation is the imposed function given by the previous expression:

$$\frac{\partial(\phi(\mathbf{x})P_g(1 - S_l(\mathbf{x}, t)))}{\partial t} - \mathrm{div}\Big(\mathbf{k}(\mathbf{x})\frac{k_{rg}(S_l(\mathbf{x}, t))}{\mu_g}(\frac{1}{2}\nabla P_g^2 - \frac{M^h P_g^2}{RT}\mathbf{g})\Big) = 0. \tag{3}$$

Then Equation (3), whose unknown is the function $P_g$, behaves in the region $S_l(\mathbf{x}, t) < 1$ as the solution of the degenerate parabolic equation $\frac{\partial u}{\partial t} - \mathrm{div}(\nabla u^m) = 0$ with $m = 2$. Such an equation, sometimes called the "porous medium equation" (in reference to a fractured medium filled by a fluid: $u$ is the fracture width, assumed to be proportional to the pressure of the fluid, whereas the permeability behaves as an increasing function of the fracture width, say $mu^{m-1}$) is degenerate in the sense that the value $u = 0$ propagates with a finite velocity. This phenomenon arises for the solution $P_g$ of Equation (3) (this is shown in numerical simulations provided at the end of this paper). As a consequence, the gas phase cannot instantaneously fill the volume released by the removal of the water phase, since the value $P_g = 0$ can only enter into this domain with a finite velocity. Let us emphasise that such a behaviour of the solution of Equations (1) does not occur in the case where $\rho_g$ is assumed to be constant, instead of $\rho_g = M^h P_g/RT$. It is no longer observed in case of low capillary pressure.

These mathematical features introduce some complexity in the numerical procedures. For example, the numerical formulation, issued from the oil reservoir engineering framework, consists in selecting $P_l$ and $S_l$ as primary unknowns for the approximate problem. This formulation is shown to be very efficient in the case of the drainage of a vertical sand column, despite of the fact that the diffusion, due to the capillary pressure, vanishes at the moving boundary between the under-saturated and the saturated zones [14]. Unfortunately, this formulation does not succeed in presence of the non-physical situation presented above, that is the apparition of vacuum zones. In order to overcome this difficulty, it is natural to modify Equations (1) in order to get rid of this nonphysical situation. Two new physical features have then to be introduced. Firstly, it is natural to let the water component, constituting the liquid phase

pass to the gaseous state, hence providing strictly positive gas pressures. Secondly, the possible dissolution of the gas component into the liquid phase has to be considered. Hence, in this paper, we now consider this miscible model, where each phase can contain both components.
Although this more complete model avoids the occurrence of the nonphysical situation precised above, the numerical approximation of this model gives rise to new difficulties, since the composition of both phases has to be prescribed by the model. The determination of these compositions is a consequence of equilibrium laws, which only apply in the under-saturated zone. Unfortunately, if one assumes that, initially, some part of the porous domain only contains pure water, the gas component conservation equation degenerates in this zone. Then the choice of the variables is essential in order to avoid divisions by zero. After elimination of the local equations, there remain only two non-local conservation equations, with two unknown functions of $\mathbf{x}, t$, called the primary unknowns. Different choices for the primary unknowns are available in the literature, some of them being different in the saturated and the under-saturated zones. The choice $P_l, S_l$, analysed in [16, 12], does not allow for solving the gas conservation equation in the saturated zone. A solution to this problem can be, as done in [3], to choose the liquid pressure, $P_l$ and the total gaseous mass density $X = \rho_g^h S_g + \rho_l^h S_l$ as main variables. Focusing on the mathematical treatment of the capillary pressure curve, we observe that, in the case of Van Genuchten-Mualem laws, the derivative of the capillary pressure with respect to the saturation tends to infinity as the saturation tends to 1; the change of variable $S_l = S_l(P_l, X)$ does not allow to get rid of this singularity.

Another possibility, presented in [1], is to extend the notion of phase saturation, allowing for negative values, and values greater than one. In another method, developed in [19], primary variables are changed, depending on the value of the saturation: they are switched when, during a time step, the gas phase appears in the saturated zone. These methods remain sensitive to capillary pressure singularities.

This paper is devoted to a new numerical procedure for approximating the solution of liquid-gas two phase miscible flow in porous media problem. This method is based on the choice of the two pressures, $P_l$ and $P_g$, as primary unknowns, whatever be the value of the saturation. We show in the paper that it leads to remarkably smooth and stable numerical approximations. Note also that such a choice is entirely compatible with the choice of finite element techniques for the space discretization, which are also shown to be efficient for the poromechanical coupling between porous medium flow and soil deformation [5, 13]. On the other hand, finite volume methods on structured grids have been used for decades in the oil engineering framework, where multi-phase multi-component flows in porous media have to be computed. This is justified by the fact that finite volume methods are natural in the framework of nonlinear hyperbolic equations. Indeed, such a framework arises in the case where the diffusion due to the capillary pressure is not large enough when, during oil production, the displacement of the fluids is mainly due to the fact that the fluids are injected and produced. In this case, upstream weighting techniques are necessary for the stability of the numerical schemes. Surprisingly, in the physical cases considered in this paper, such upstream weighting numerical techniques remain necessary due to vanishing diffusion effects within the saturated zone [7]. In order to obtain a method which can gather the advantages of the finite element and finite volume methods, we propose here a finite volume formulation suited to unstructured general meshes. This method is based on a technique developed for heterogeneous anisotropic diffusion equation [11].

This paper is structured as follows. In section 2, we present the model for diffusion-dissolution liquid-gas flow in a porous medium. Then, in section 3, we present the discretization method. Finally, in section 4, we show the efficiency and the accuracy of the formulation, on typical test case used in order to simulate the storage of nuclear waste. In particular, we consider the case where it is used as a regularisation method for the model (1).

## 2. Physical and mathematical model

We now present a standard model for miscible two phase flow in a porous medium. The density $\rho_p^c$ of each component $c = w, h$ in each phase $p = l, g$ is linked to the density of the phase $p = l, g$ by the relation:

$$\rho_p = \rho_p^h + \rho_p^w. \tag{4}$$

The molar concentration $C_p$ of phase $p = l, g$, the molar concentration $C_p^c$ and the molar fraction $X_p^c$ of component $c = w, h$ in phase $p = l, g$ are respectively defined by

$$C_p^c = \frac{\rho_p^c}{M^c},\ C_p = C_p^h + C_p^w \text{ and } X_p^c = \frac{C_p^c}{C_p}, \tag{5}$$

where $M^c$ denotes the molar mass of component $c$. As done in the introduction of this paper, the liquid saturation $S_l$ is chosen as variable for the relative permeability $k_{rp}$ and capillary pressure $P_c$ curves, whereas the gas saturation $S_g$ satisfies

$$S_l + S_g = 1. \tag{6}$$

The liquid phase and gas phase pressures are linked with $S_l$ by the relation

$$P_g - P_l = P_c(S_l). \tag{7}$$

The mass conservation equations of the two components $c = w, h$ read:

$$\begin{cases} \dfrac{\partial m_l^w}{\partial t} + \dfrac{\partial m_g^w}{\partial t} & + \operatorname{div}\left(\rho_l^w \dfrac{\mathbf{F}_l}{\rho_l} + \rho_g^w \dfrac{\mathbf{F}_g}{\rho_g} + \mathbf{J}_l^w + \mathbf{J}_g^w\right) = 0 \\ \dfrac{\partial m_l^h}{\partial t} + \dfrac{\partial m_g^h}{\partial t} & + \operatorname{div}\left(\rho_l^h \dfrac{\mathbf{F}_l}{\rho_l} + \rho_g^h \dfrac{\mathbf{F}_g}{\rho_g} + \mathbf{J}_l^h + \mathbf{J}_g^h\right) = 0, \end{cases} \tag{8}$$

with $m_p^c = \phi \rho_p^c S_p$. In (8), we denote by $\mathbf{F}_p$ the flux given by Darcy's law:

$$\frac{\mathbf{F}_p}{\rho_p} = -\frac{\mathbf{k} k_{rp}}{\mu_p}(\nabla P_p - \rho_p \mathbf{g}), \tag{9}$$

where we denote by $\mathbf{g}$ the gravity acceleration. We define $\mathbf{J}_p^c$ as the diffusive flux given by Fick's law [6, 15]:

$$\mathbf{J}_g^w = -\phi M^w S_g D_g^w C_g \nabla X_g^w, \;\; \mathbf{J}_g^h = -\phi M^h S_g D_g^h C_g \nabla X_g^h, \;\; \mathbf{J}_l^w = -\phi M^w S_l D_l^w C_l \nabla X_l^w, \;\; \mathbf{J}_l^h = -\phi M^h S_l D_l^h C_l \nabla X_l^h.$$

Since, in the applications under consideration in this paper, Fick's flow of water in the liquid phase is negligible in front of the liquid phase Darcy flow, we set in (8):

$$\mathbf{J}_g^w = -\phi M^w S_g D_g^w C_g \nabla X_g^w, \;\; \mathbf{J}_g^h = -\phi M^h S_g D_g^h C_g \nabla X_g^h, \;\; \mathbf{J}_l^w = 0, \;\; \mathbf{J}_l^h = -\phi M^h S_l D_l^h C_l \nabla X_l^h. \tag{10}$$

In order to close the system, equilibrium laws for components $c = w, h$ are required. Since our concern is to focus on gas injection or on the regularisation of immiscible two-phase flow, we now assume that $\rho_g^w = 0$, and we are no longer accounting for the water component within the gaseous phase. We assume that the equilibrium of the gas component $h$ between the two phases is prescribed by Henry's law, which can be expressed by:

$$\left(\rho_l^h = H M^h P_g \text{ and } S_l < 1\right) \text{ or } \left(\rho_l^h \leq H M^h P_l \text{ and } S_l = 1\right), \tag{11}$$

denoting by $H$ Henry's constant at the temperature of the domain (supposed to be constant in space and time) and assuming that $P_c(1) = 0$.

Let us now rewrite the system of all preceding equations, remarking that, in the saturated zone $S_l = 1$, all terms of System (8) which depend on $P_g$ are multiplied by $S_g = 0$ or $k_{rg}(1) = 0$. Hence $P_g$, which is linked to $\rho_l^h$ in the region $S_l < 1$ by (11), can be freely defined in the region $S_l = 1$. Hence we choose to set

$$P_g = \frac{\rho_l^h}{H M^h} \text{ in both cases } S_l = 1, \text{ and } S_l < 1. \tag{12}$$

Then, from (12), the relation $C_l^h = H P_g$ holds in both saturated and under-saturated zones and from (11), the inequality $P_g \leq P_l$ holds in the saturated zone $S_l = 1$. Therefore, $P_g$ is continuous across the transition area between the saturated and the under-saturated zones, and we can write the relation

$$S_l = C(P_g - P_l), \tag{13}$$

where, as in the introduction of this paper, the capacity function $C(P)$ is defined as the reciprocal function to the capillary pressure for $P \geq 0$ and equal to 1 for $P \leq 0$. This function $C(P)$ is then in some cases differentiable at

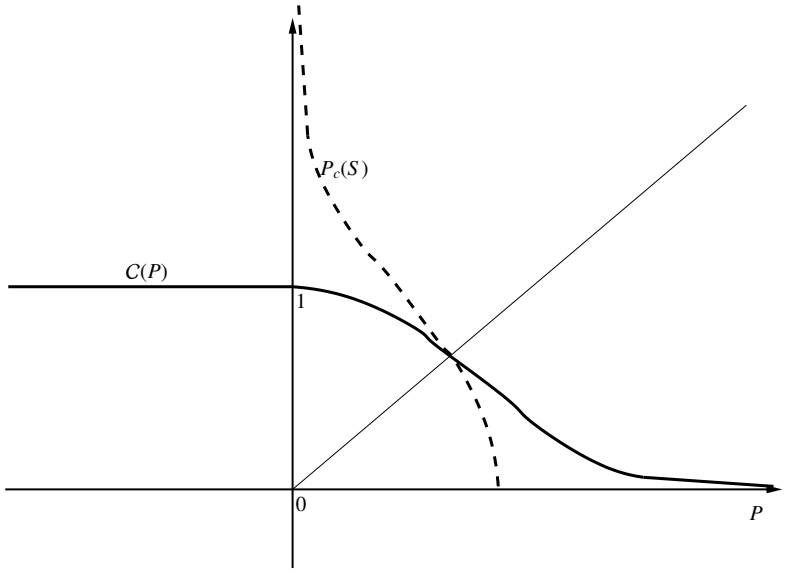


Figure 1: Capacity function

point $P = 0$ (this holds for example in the case of Van Genuchten's functions, see Figure 1). Hence the system of all equations, from (4) to (11), resumes to the following system of equations, with respect to the two unknowns $P_l$ and $P_g$:

$$\left\{ \begin{array}{ll} \dfrac{\partial \phi A^w(P_l,P_g)}{\partial t} & - \operatorname{div}\Big(\mathbf{k} B_l^w(P_l,P_g)(\nabla P_l - \rho_l \mathbf{g})\Big) = 0 \\ \dfrac{\partial \phi A^h(P_l,P_g)}{\partial t} & - \operatorname{div}\Big(\mathbf{k} B_l^h(P_l,P_g)(\nabla P_l - \rho_l \mathbf{g}) + \mathbf{k} B_g^h(P_l,P_g)(\nabla P_g - \rho_g(P_g)\mathbf{g}) + \phi D_l^h(P_l,P_g)\nabla P_g\Big) = 0, \end{array} \right. \tag{14}$$

where

$$\begin{array}{l} A^w(P_l,P_g) = \rho_l C(P_g - P_l),\ B_l^w(P_l,P_g) = \rho_l \dfrac{k_{rl}(C(P_g - P_l))}{\mu_l}, \\ \rho_g(P_g) = \dfrac{M^h P_g}{RT},\ A^h(P_l,P_g) = \rho_g(P_g)(1 - C(P_g - P_l)) + HM^h P_g C(P_g - P_l), \\ B_l^h(P_l,P_g) = HM^h P_g \dfrac{k_{rl}(C(P_g - P_l))}{\mu_l},\ B_g^h(P_l,P_g) = \rho_g(P_g)\dfrac{k_{rg}(C(P_g - P_l))}{\mu_g}, \\ D_l^h(P_l,P_g) = M^h C(P_g - P_l) D_l^h \dfrac{\rho_l^w}{M^w} H. \end{array} \tag{15}$$

An advantage of this formulation, from the point of view of numerical implementation, is that the coefficient $\partial A^h(P_l,P_g)/\partial P_g$ does no longer vanish in the saturated zone, where it is equal to $HM^h$. If we assume that $D_l^h > 0$, we also get that the coefficient of $\nabla P_g$ does not vanish in the saturated zone, since it is equal to $D_l^h HM^h > 0$. Nevertheless, if we approximate the immiscible problem (1) by System (14), using a small value for $H$ and letting $D_l^h = 0$, the coefficient of $\nabla P_g$ vanishes in the saturated zone (this is the approximation method used in the third example in section 4).

## 3. The numerical scheme

Our aim is to extend to the system (14), the SUSHI scheme (Scheme Using Stabilisation and Hybrid Interfaces), presented in [11, 10, 11, 9] in the case of a heterogeneous and anisotropic pure diffusion problem. This scheme leads to the approximation, for a scalar field $u$ defined on the domain, of the flux $-\int_\sigma \mathbf{k}\nabla u.\mathbf{n}_{K,\sigma} d\gamma$, in the case where the domain $\Omega$ has been partitioned into a mesh $\mathcal{M}$ (for example, triangles, quadrangles,...), $K$ is one element of the mesh

$\mathcal{M}$ and $\sigma$ is an edge of $K$ (see figure 2). The continuous field $u$ is approximated by discrete values $u_K$, approximating $u$ at given points $\mathbf{x}_K \in K$ (in the case of triangles, we choose here the barycentre of the triangle, but this is not mandatory, and we could as well choose the circumcentre for example), and $u_\sigma$, approximating $u$ at the barycentre $\mathbf{x}_\sigma$ of $\sigma$.

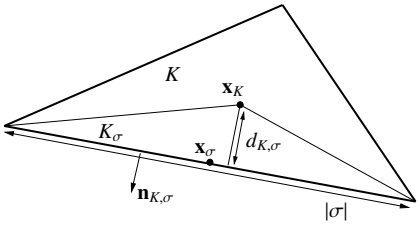


Figure 2: Geometrical description of control volume $K$

First, an approximate gradient of $u$ in $K$ is reconstructed, thanks to the relation

$$\nabla_K U_K = \frac{1}{|K|} \sum_{\sigma \in \mathcal{E}_K} |\sigma|(u_\sigma - u_K)\mathbf{n}_{K,\sigma},$$

where $U_K = (u_K, (u_\sigma)_{\sigma \in \mathcal{E}_K})$. Then an approximate gradient is reconstructed in the cone $K_\sigma$ with vertex $\mathbf{x}_K$ and basis $\sigma$,

$$\nabla_{K,\sigma} U_K = \nabla_K U_K + \frac{\beta_K}{d_{K,\sigma}} \left(u_\sigma - u_K - \nabla_K U_K \cdot (\mathbf{x}_\sigma - \mathbf{x}_K)\right) \mathbf{n}_{K,\sigma},$$

where $\beta_K$ is a parameter which is equal to $\sqrt{d}$ for getting back the 5-point scheme in the case of rectangular meshes. In case of highly distorted meshes, this parameter can be adjusted in order to prevent from oscillations [2]. We assume that the permeability $\mathbf{k}$ takes the constant value $\mathbf{k}_K$ in $K$.
Then $(F_{K,\sigma}(U_K))_{\sigma \in \mathcal{E}_K}$ is defined as the unique family of values such that the following relation holds

$$\sum_{\sigma \in \mathcal{E}_K} F_{K,\sigma}(U_K)(v_\sigma - v_K) = \sum_{\sigma \in \mathcal{E}_K} |K_\sigma|\, \mathbf{k}_K \nabla_{K,\sigma} U_K \cdot \nabla_{K,\sigma} V_K, \quad \forall V_K = (v_K, (v_\sigma)_{\sigma \in \mathcal{E}_K}) \in \mathbb{R}^{1+\#\mathcal{E}_K}. \tag{16}$$

Note that, in (16), the value $|K_\sigma|$, measure of the cone $K_\sigma$, is given by $\frac{|\sigma| d_{K,\sigma}}{d}$, where $d$ is the space dimension. It results from (16) an expression of $F_{K,\sigma}$ under the form:

$$F_{K,\sigma}(U_K) = \sum_{\sigma' \in \mathcal{E}_K} M_K^{\sigma,\sigma'}(u_K - u_{\sigma'}) \tag{17}$$

where the local matrices $(M_K^{\sigma,\sigma'})_{\sigma,\sigma' \in \mathcal{E}_K}$ are symmetric and positive. In the case of a monophasic diffusion problem, the balance of the diffusion terms in the control volume $K$ is equal to $\sum_{\sigma \in \mathcal{E}_K} F_{K,\sigma}(U_K)$, and the continuity equation $F_{K,\sigma}(U_K) + F_{L,\sigma}(U_L) = 0$ is requested for all common interface $\sigma$ to two neighbouring control volumes $K$ and $L$.
Since the scheme (14) also contains pure diffusion terms, we also need to have an approximate of $-\int_\sigma \nabla u.\mathbf{n}_{K,\sigma} d\gamma$ (this term no longer includes the permeability matrix $\mathbf{k}$). Hence we similarly define the family $(G_{K,\sigma}(U_K))_{\sigma \in \mathcal{E}_K}$ as the unique family of values such that

$$\sum_{\sigma \in \mathcal{E}_K} G_{K,\sigma}(U_K)(v_\sigma - v_K) = \sum_{\sigma \in \mathcal{E}_K} |K_\sigma|\, \nabla_{K,\sigma} U_K \cdot \nabla_{K,\sigma} V_K, \quad \forall V_K = (v_K, (v_\sigma)_{\sigma \in \mathcal{E}_K}) \in \mathbb{R}^{1+\#\mathcal{E}_K}, \tag{18}$$

which provides, for the expression of $G_{K,\sigma}(U_K)$, an expression similar to (17).
We may now use these functions $F_{K,\sigma}$ and $G_{K,\sigma}$ for defining the approximation of (14).
We first use, for the time discretization, an Euler backward (implicit) scheme, using the time step $\Delta t > 0$. The discrete unknowns are now the values $P_{l,K}$, $P_{g,K}$ approximating at the end of the time step the liquid and gas pressures at point $\mathbf{x}_K$, and the values $P_{l,\sigma}$, $P_{g,\sigma}$ approximating at the end of the time step the liquid and gas pressures at point $\mathbf{x}_\sigma$. The approximation of the term

$$\overline{F}_{l,K,\sigma}^{w} = -\int_\sigma \mathbf{k} B_l^w(P_l, P_g)(\nabla P_l - \rho_l \mathbf{g}).\mathbf{n}_{K,\sigma} d\gamma$$

is then given, in the case where $\sigma$ is a common interface between two neighbouring control volumes $K$ and $L$, by

$$F^w_{l,K,\sigma} = B^w_l(P_l, P_g)^{\rm ups}_{K,L}\,(F_{K,\sigma}(P_{l,K}, (P_{l,\sigma})_{\sigma\in\mathcal{E}_K}) - |\sigma|\rho_l \mathbf{k}_K \mathbf{g}\cdot\mathbf{n}_{K,\sigma}), \tag{19}$$

where the upstream weighting expression $B^w_l(P_l, P_g)^{\rm ups}_{K,L}$ is defined by

$$\begin{array}{ll} B^w_l(P_l, P_g)^{\rm ups}_{K,L} = B^w_l(P_{l,K}, P_{g,K}) & \text{if} \quad (F_{K,\sigma}(P_{l,K}, (P_{l,\sigma})_{\sigma\in\mathcal{E}_K}) - \mathbf{k}_K|\sigma|\rho_l\mathbf{g}\cdot\mathbf{n}_{K,\sigma}) \geq 0 \\ B^w_l(P_l, P_g)^{\rm ups}_{K,L} = B^w_l(P_{l,L}, P_{g,L}) & \text{otherwise.} \end{array}$$

The continuity equation

$$F_{K,\sigma}(P_{l,K}, (P_{l,\sigma})_{\sigma\in\mathcal{E}_K}) - |\sigma|\rho_l\mathbf{k}_K\mathbf{g}\cdot\mathbf{n}_{K,\sigma} + F_{L,\sigma}(P_{l,L}, (P_{l,\sigma})_{\sigma\in\mathcal{E}_L}) - |\sigma|\rho_l\mathbf{k}_L\mathbf{g}\cdot\mathbf{n}_{L,\sigma} = 0, \tag{20}$$

is also solved. It could be possible to consider different expressions for the continuity equation (20), involving for example nonlinear terms at the interface. The advantage of (20) is that it remains linear and does not degenerate if a phase disappear. Note also that a consequence of (20) and of the definition (19) of $F^w_{l,K,\sigma}$ is the continuity equation

$$F^w_{l,K,\sigma} + F^w_{l,L,\sigma} = 0.$$

Similar expressions are derived for the terms involved in the conservation of the gas component. The upstream weighting definition for $B^h_l(P_l, P_g)$ is again depending on the sign of the expression $F_{K,\sigma}(P_{l,K}, (P_{l,\sigma})_{\sigma\in\mathcal{E}_K}) - \mathbf{k}_K|\sigma|\rho_l\mathbf{g}\cdot\mathbf{n}_{K,\sigma}$, whereas the upstream weighting definition for $B^h_g(P_l, P_g)$ is depending on the sign of the expression $F_{K,\sigma}(P_{g,K}, (P_{g,\sigma})_{\sigma\in\mathcal{E}_K}) - \mathbf{k}_K|\sigma|\rho_g(P_{g,K})\mathbf{g}\cdot\mathbf{n}_{K,\sigma}$. Finally, the diffusion term

$$\overline{D}^h_{l,K,\sigma} = -\int_\sigma \phi D^h_l(P_l, P_g)\nabla P_g.\mathbf{n}_{K,\sigma} d\gamma$$

is approximated by

$$D^h_{l,K,\sigma} = \frac{1}{2}(\phi_K D^h_l(P_{l,K}, P_{g,K}) G_{K,\sigma}(P_{g,K}, (P_{g,\sigma})_{\sigma\in\mathcal{E}_K}) - \phi_L D^h_l(P_{l,L}, P_{g,L}) G_{L,\sigma}(P_{g,L}, (P_{g,\sigma})_{\sigma\in\mathcal{E}_L}))\,.$$

Note that all terms $A^c(P_l, P_g)$, $B^c_p(P_l, P_g)$, $D^h_l(P_l, P_g)$ involve some functions which depend on the rock type (capacity function, relative permeabilities). Hence a dependence with respect to the control volume has not been written for the sake of simpler notations. The scheme can then be written, using the superscript "$-$" for expressing values at the beginning of the time step:

$$\begin{array}{ll}
\dfrac{|K|\phi_K}{\Delta t}(A^w(P_{l,K}, P_{g,K}) - A^w(P^-_{l,K}, P^-_{g,K})) + \displaystyle\sum_{\sigma\in\mathcal{E}_K} F^w_{l,K,\sigma} & = 0,\ \forall K\in\mathcal{M} \\
\dfrac{|K|\phi_K}{\Delta t}(A^h(P_{l,K}, P_{g,K}) - A^h(P^-_{l,K}, P^-_{g,K})) + \displaystyle\sum_{\sigma\in\mathcal{E}_K} (F^h_{l,K,\sigma} + F^h_{g,K,\sigma} + D^h_{l,K,\sigma}) & = 0,\ \forall K\in\mathcal{M} \\
F_{K,\sigma}(P_{l,K}, (P_{l,\sigma})_{\sigma\in\mathcal{E}_K}) - |\sigma|\rho_l\mathbf{k}_K\mathbf{g}\cdot\mathbf{n}_{K,\sigma} + F_{L,\sigma}(P_{l,L}, (P_{l,\sigma})_{\sigma\in\mathcal{E}_L}) - |\sigma|\rho_l\mathbf{k}_L\mathbf{g}\cdot\mathbf{n}_{L,\sigma} & = 0,\ \forall\sigma\in\mathcal{E}_{\rm int} \\
F_{K,\sigma}(P_{g,K}, (P_{g,\sigma})_{\sigma\in\mathcal{E}_K}) - |\sigma|\rho_g(P_{g,K})\mathbf{k}_K\mathbf{g}\cdot\mathbf{n}_{K,\sigma} + F_{L,\sigma}(P_{g,L}, (P_{g,\sigma})_{\sigma\in\mathcal{E}_L}) - |\sigma|\rho_g(P_{g,L})\mathbf{k}_L\mathbf{g}\cdot\mathbf{n}_{L,\sigma} & = 0,\ \forall\sigma\in\mathcal{E}_{\rm int}.
\end{array} \tag{21}$$

Hence we get a system of nonlinear discrete equations. We approximate its solution, using the exact Newton's method (taking advantage of the fact that all functions are given by an analytical expression in the numerical examples considered in this paper). Since our aim is to focus on the schemes, we only used direct Gaussian elimination solvers. The convergence criterion is tuned such that an average number of 2 or 3 iterations is performed at each time step. This numerical scheme has been implemented within Code_Aster [8], which is an open source finite element code used for research/development purposes in EDF.

## 4. Numerical results

We present in this paper three applications of the use of Scheme (21). The first one is a benchmark problem proposed by F. Smaï et al. [17]; the second one is a two-dimensional extension of this benchmark problem. The third one corresponds to the use of Scheme (21) for regularising the immiscible problem described in the introduction of this paper.

*4.1. Test 1: Gas injection in a saturated porous media in one dimension*

The aim of the test proposed in [17] is to check the numerical schemes in the case of production of hydrogen due to acid attack of metallic containers. The production of hydrogen is represented by a mass injection rate $Q$ during the first 500 000 years, equal to 0 after, at the left boundary of a one dimension domain $\Omega = ]0\text{m}; 200\text{m}[$ (the section of the domain is assumed to be equal to 1 $\text{m}^2$), initially saturated with pure water. We consider two cases:

1. the first one is that provided in [17], where $Q = 1.766\ 10^{-13}\ \text{kg.m}^{-2}.\text{s}^{-1} = 5.57\ 10^{-6}\ \text{kg.m}^{-2}.\text{year}^{-1}$,
2. the second case, motivated by additional interesting physical phenomena, is given by $Q = 4.76\ 10^{-13}\ \text{kg.m}^{-2}.\text{s}^{-1} = 1.50\ 10^{-5}\ \text{kg.m}^{-2}.\text{year}^{-1}$.

The water flux is assumed to be null at the left boundary. At the right boundary, the value $10^6$ Pa is imposed for the liquid pressure and it is assumed that there is no free nor dissolved gas.

For this test we use the Van Genuchten-Mualem model, defined by the values of the parameters $P_r$, $S_{lr}$, $S_{gr}$, $m$ and $n$, for expressing the capillary pressure and the relative permeability:

$$S_{le} = \frac{S_l - S_{lr}}{1 - S_{lr} - S_{gr}},\quad P_c = P_r(S_{le}^{-\frac{1}{m}} - 1)^{\frac{1}{n}},\quad k_{rl} = \sqrt{S_{le}}(1 - (1 - S_{le}^{\frac{1}{m}})^m)^2,\quad k_{rg} = \sqrt{(1 - S_{le})}(1 - S_{le}^{\frac{1}{m}})^{2m}. \tag{22}$$

The parameters involved by (22), as well as the physical data and fluid characteristics are resumed in Table 1.

| Porous medium | | Characteristics of fluids | |
|---|---|---|---|
| Parameter | Value | Parameter | Value |
| $\mathbf{k}(\text{m}^2)$ | $5\ 10^{-20}$ | $D_l^h\ (\text{m}^2.\text{s}^{-1})$ | $3\ 10^{-9}$ |
| $\phi$ | 0.15 | $\mu_l$ (Pa.s) | $10^{-3}$ |
| $P_r$ (Pa) | $2\ 10^6$ | $\mu_g$ (Pa.s) | $9\ 10^{-6}$ |
| $n$ | 1.49 | $H$ ( $\text{mol.Pa}^{-1}.\text{m}^{-3}$) | $7.65\ 10^{-6}$ |
| $S_{lr}$ | 0.4 | $M^w\ (\text{kg.mol}^{-1})$ | $18\ 10^{-3}$ |
| $S_{gr}$ | 0 | $M^h\ (\text{kg.mol}^{-1})$ | $2\ 10^{-3}$ |
| $m$ | $1 - \frac{1}{n}$ | $\rho_l(\text{kg.m}^{-3}\ )$ | $10^3$ |

Table 1: Data of benchmark problem [17]

The time variable $t$ belongs to the range $]0, 10^6[$ years, discretized in 556 time steps whose size is between 1 day at the beginning of the simulation and 16 666 years at its end.

Figure 3 presents the profiles of the gas pressure at different times, in the two cases. We observe that, in Case 1, the gas pressure mainly behaves as expected, in the sense that, at each location, it increases with respect to the time, except for the small values of $x$ at $t = 500\,000$ years, where this pressure is smaller than that obtained for $t = 100\,000$ years. This behaviour is more clearly observed in Case 2: the gas pressure is lower for $t = 500\,000$ years than that obtained for $t = 100\,000$ years, in almost the whole region $S_g > 0$. This is due to the fact that the main part of the volume needed for the gas phase is occupied at $t = 100\,000$ years. The increase of this volume imposes an outward water rate at the right boundary of the domain, and therefore a strictly negative gradient of the liquid pressure along the domain. When the total volume of the gaseous phase has reached its maximum value, there is no further need for a large liquid flow from the left to the right of the domain. Then no negative gradient for the liquid pressure is necessary, and the liquid pressure tends to the constant value imposed at the right boundary, whereas a small gas pressure gradient remains necessary in the zone $S_l < 1$ for transporting the injected gas to the right boundary.

We present in Figure 4 the values of the pressures of both phases at the left boundary of the domain, with respect to the time variable, only for Case 1 (the results for Case 2 show the same behavior). After the end of the gas injection (i.e., for $t > 500\,000$ years), the gas component is progressively eliminated thanks to the value 0 imposed at the right boundary. Hence the gas phase disappears in the domain, which imposes a flux of water, from the right to the left, in order to replace the volume occupied by the gas phase. This induces a positive gradient to the liquid pressure. Hence the liquid pressure must become smaller at the left boundary than that imposed at the right boundary, in order to get a positive gradient. This behaviour finishes when the liquid saturation is again equal to 1 in all the domain (in Figure 4,

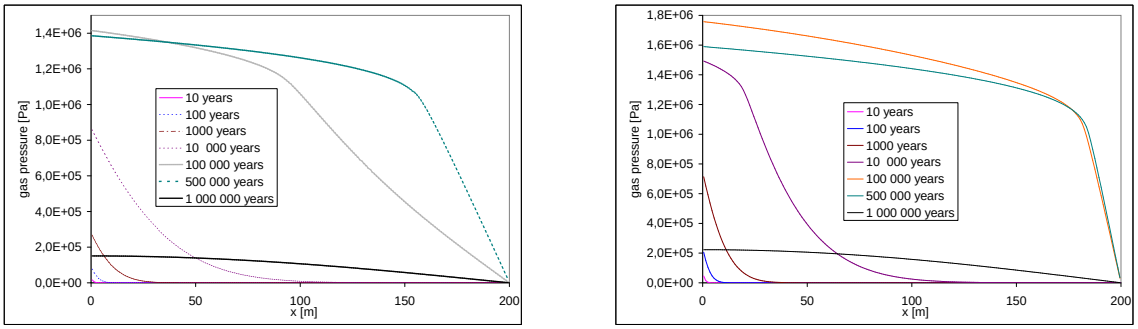


Figure 3: Gas pressure at different times (left: case 1, right: case 2).

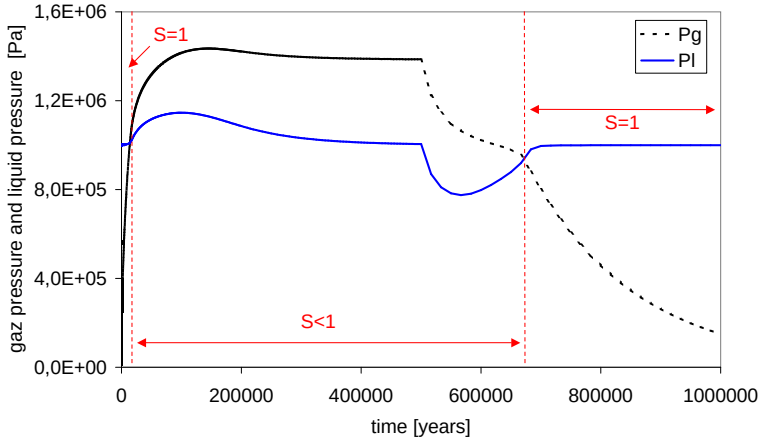


Figure 4: Gas pressure and liquid pressure at the left boundary of the domain in Case 1.

the indications $S = 1$ or $S < 1$ respectively mean that $S_l(0,t) = 1$ or $S_l(0,t) < 1$). We recall that the values of the gas pressure, which are lower than that of the liquid pressure must be interpreted as a gas concentration in the liquid phase.

Figure 5 presents the liquid saturation obtained at different times, only for Case 1 (the results for Case 2 are again similar), computed using the capacity function from the pressure values of both phases. We observe that the location of the free boundary is an easy consequence of the discrete conservation equations. Figure 6 presents the outward rates (liquid and gas) at the right boundary, with respect to time. The inversion of the sense of the water flow after the end of injection is clearly put in evidence.

### *4.2. Test 2: Gas injection in a saturated porous media in two dimensions*

This test is a two dimensional adaptation of the benchmark problem presented in section 4.1. We assume that the domain is horizontal with thickness 1 m (Figure 7).

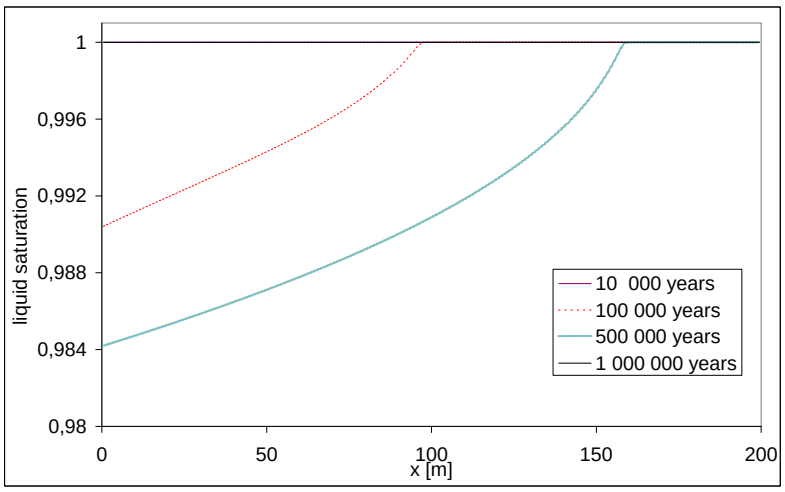


Figure 5: Saturation at different times in Case 1.

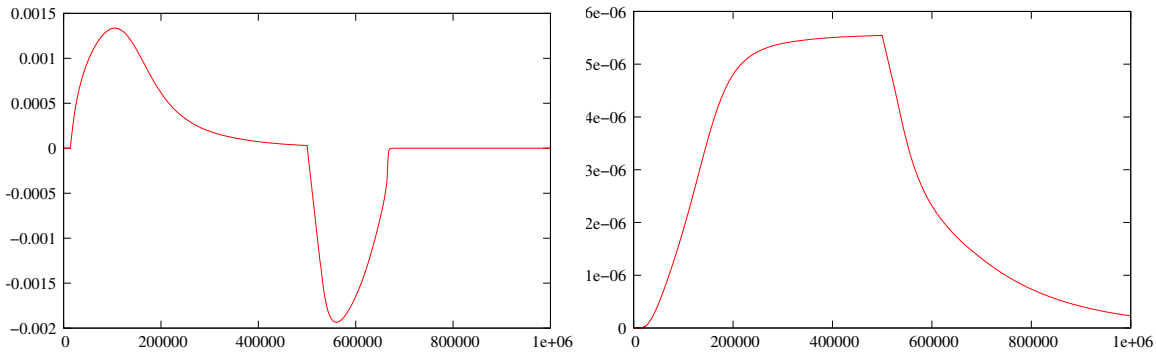


Figure 6: Outward liquid flux (left) and gas flux (right) at right boundary, kg/m$^2$/year, with respect to time, years, Case 1.

The porous medium and fluid data are again given by (22) and Table 1. The domain, depicted in left part of Figure 7, is initially saturated with pure water. The value $10^6$ Pa is imposed to the liquid pressure in the upper right corner of the domain, which is assumed to be free of gas component. The total gas rate, injected in the lower left corner of the domain, is equal to 1.76 $10^{-11}$ kg.m$^{-2}$.s$^{-1}$ during the first 500 000 years. The other boundaries are assumed to be impervious. We use a triangular mesh with 1632 elements (right part of Figure 7).
The time interval is discretized in 466 time steps, whose size varies between 1 day and 16 666 years.
Figure 8 shows the gas pressure and saturation at different times into the domain. It shows a similar behaviour in 2D to that observed in 1D. The red colour in the saturation field shows the saturated zone, which corresponds to a gas pressure lower than the liquid pressure. The boundary between the saturated and the under-saturated zone exactly corresponds to the isovalue line $P_g = 10^6$ Pa. This test confirms that the numerical scheme is suited for handling this problem in 2D (further tests will be performed in 3D).

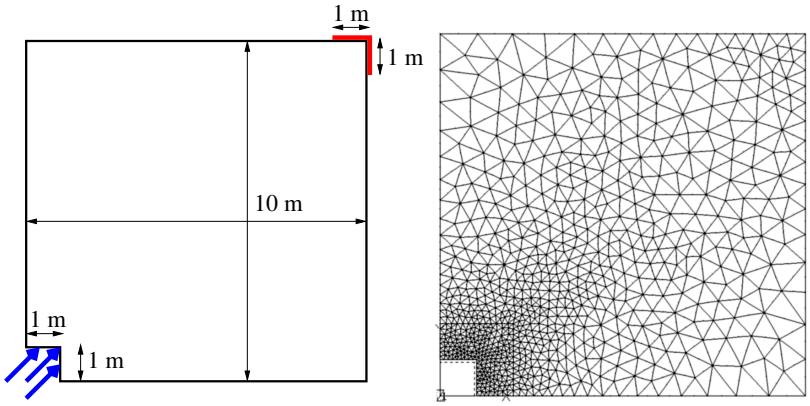


Figure 7: Dimensions of the domain (left), mesh used for the simulation (right)

| Porous medium M1 | | Porous medium M2 | | Characteristics of fluids | |
|---|---|---|---|---|---|
| Parameter | Value | Parameter | Value | Parameter | Value |
| $\mathbf{k}$ ($m^2$) | $10^{-20}$ | $\mathbf{k}$ ($m^2$) | $10^{-19}$ | $D_l^h$ ($m^2.s^{-1}$) | 0 |
| $\phi$ | 0.3 | $\phi$ | 0.05 | $H$ ($mol.Pa^{-1}.m^{-3}$) | $3.8\ 10^{-10}$ |
| $A$ (Pa) | $1.5\ 10^6$ | $A$ (Pa) | $10\ 10^6$ | $\mu_l$ (Pa.s) | $10^{-3}$ |
| $B$ | 0.06 | $B$ | 0.412 | $\mu_g$ (Pa.s) | $1.8\ 10^{-5}$ |
| $a$ | 0.25 | $a$ | 1 | $\rho_l$ ($kg.m^{-3}$ ) | $10^3$ |
| $b$ | 16.67 | $b$ | 2.429 | $M^w$ ($kg.mol^{-1}$) | $18\ 10^{-3}$ |
| $c$ | 1.88 | $c$ | 1.176 | $M^h$ ($kg.mol^{-1}$) | $28.96\ 10^{-3}$ |
| $d$ | 0.5 | $d$ | 1 | | |

Table 2: Physical data

### *4.3. Test 3: approximation of immiscible two-phase flow in one dimension*

This test is firstly dedicated to numerically validate the analysis of the behaviour of the solution, proposed in the introduction of this paper, and secondly to show that the numerical method presented in this paper leads to an easy numerical approximation of the problem. The data are those provided by [4]. We consider the 1D domain $]0,1[$ m (assumed to have a section equal to 1 $m^2$). It is composed of two materials, M1 and M2, as shown in Figure 9.

The capillary pressure and the relative permeabilities are defined by

$$S_l(P_c) = \left(1 + \left(\frac{P_c}{A}\right)^{1/(1-B)}\right)^{-B},\ k_{rl}(S_l) = \left(1 + a(S_l^{-b} - 1)^c\right)^{-d},\ k_{rg}(S_l) = (1 - S_l)^2(1 - S_l^{5/3}), \tag{23}$$

where the parameters $A, B, a, b, c, d$ and the porous medium data are provided by Table 2.

We assume no flow boundary conditions at the left and right parts of the domain. We consider the following two cases for the initial conditions:

Case 1:

$$\begin{cases} S_l = 0.77,\ P_g = 10^5 \text{ Pa and } P_l = P_g - P_c(S_l) & \text{in M1,} \\ S_l = 1,\ P_g = 0 \text{ Pa and } P_l = 10^5 \text{ Pa} & \text{in M2.} \end{cases} \tag{24}$$

Case 2:

$$\begin{cases} S_l = 0.77,\ P_g = 10^5 \text{ Pa and } P_l = P_g - P_c(S_l) & \text{in M1,} \\ S_l = 1,\ P_g = 10^5 \text{ Pa and } P_l = 10^5 \text{ Pa} & \text{in M2.} \end{cases} \tag{25}$$

A 1D mesh with 200 elements has been used, and the time period $[0, 10^{11}]$ s (3169 years) is considered. A number of 3730 time steps is required, for both initial data cases, whereas the size of the time steps varies from .1 s to 5. $10^6$ s (arbitrary above limit) during the computation.

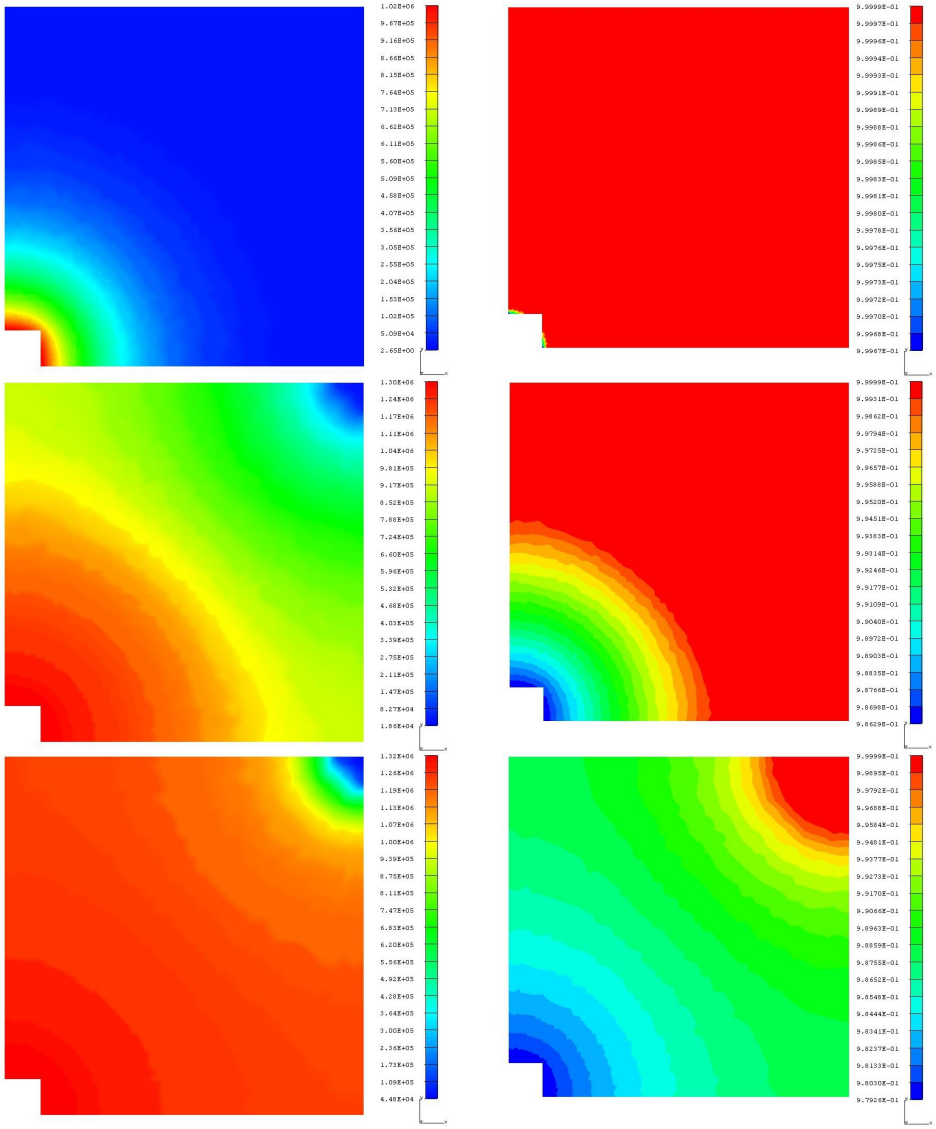

Figure 8: Gas pressure (left) and liquid saturation (right) at different times: top 50 years, middle 1 000 years, bottom 10 000 years

The gas pressure is shown in Figure 10 for Case 1 and in Figure 11 for Case 2. Since, in Case 2, the amount of dissolved gas in water is very small accounting for the value of $H$ provided by Table 2, one could expect that both cases would lead to close results. This is indeed what we observed, since, for the other variables (liquid pressure and saturation, total mass of gas per unit of porous medium volume), both cases lead to identical results up to the plotting precision due to the fact that the amount of dissolved gas is very small. So only one figure is proposed for the liquid pressure (Figure 12), the liquid saturation (Figure 13) and the global density of gas (defined by the quantity $m_l^h + m_g^h$ of the balance equation (8)) is plotted in Figure 14.

We observe that the numerical results follow the analysis developped in the introduction of this paper. In a first period ($t < 10^5$s), water flows from region M2 to region M1 (see Figure 13). This leads to a reduction of the porous volume occupied by the gas phase in M1, and provides an increase in the value of the gas pressure (Figures 10 and 11). The volume which was previously occupied by the water phase in M2 cannot be instantaneously filled by the gas phase present in M1. In case 1 (Figure 11), an exact vacuum is observed in M2, whereas in case 2, the main part of

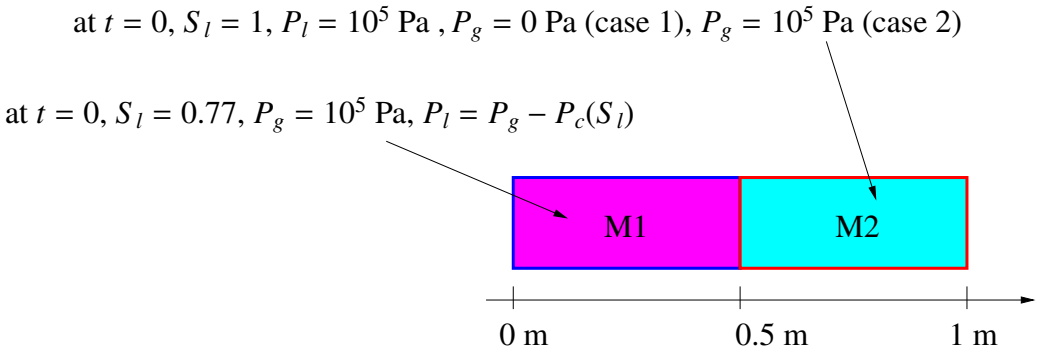


Figure 9: The geometry.

the dissolved gas pass to the gas phase. But, since in case 2, the amound of dissolved gas is very small, the pressures obtained in the gas phase are very low and close to 0 in the case where $1-S_l$ is large enough. For $1-S_l \to 0$ as $x \to 1$, we naturally observe in Figure 11 that $P_g \to 10^5$, which is equal to the initial equilibrium pressure of the dissolved gas. Let us notice that the location in M2 of the boundary between the regions $S_l < 1$ to $S_l = 1$ is more precisely assessed in Figure 11 by the location at which the gas pressure tends to its initial value, about 0.6 m for $t = 100$ s and 0.95s for $t = 1000$ s, than by Figure 13. We observe that this location moves with a finite velocity, which is expected for the solution of (2), similar to Richards equation.

At time $t = 20000$ s, the gas pressures obtained in both cases are still different but already very close. For larger times, the pressures obtained in both cases become undistinguishable. We then observe in M2, for $t = 10^6$, $10^7$ and $10^8$ s, the characteristic shape corresponding to the porous medium equation $\partial u/\partial t - \partial^2(u^m)/\partial x^2 = 0$ with $m = 2$, that is a finite slope at $u = 0$. At large times, the gas pressure becomes constant, which is expected since the gas phase is mobile in the whole domain. Since the volume occupied by the gas phase at the end of the simulation in M1 and M2 is the same as the one which was initially occupied by the gas phase in M1, the final pressure is about $10^5$ Pa, which is the same as the initial one (again, even in case 2, the amount of dissolved gas does not significantly modify this quantity).

Let us now comment the results obtained for the liquid pressure in Figure 12 and the liquid saturation in Figure 13. This pressure is highly negative, which corresponds to traction cases observed for materials such as clays and cement concrete. We must recall that the pressures are linked to the free energy of the water phase, which accounts for all types of interactions with the solid phase (such interactions being particularly complex in the case of clays), and Darcy's law provides a dissipation mechanism compatible with the second principle of thermodynamics [6]. We observe that, at short times, the variation of the saturation is greater in region M2 than in region M1, due to the contrast between the porosity values. At all times, the saturation presents a discontinuity in $x = 0.5$, due to the fact that, since both phases flow at this location, the gas and the liquid pressures must remain continuous. Therefore, the saturation must respect the equation $P_c^{(1)}(S_l^{(1)}(0.5,t)) = P_c^{(2)}(S_l^{(2)}(0.5,t))$, where upper indices (1) and (2) denote the values and functions respectively available in regions M1 and M2, at all times $t > 0$, which leads to different left and right limits of the saturation in $x = 0.5$. At large times, the liquid pressure becomes constant, which is expected since the water phase is mobile in the whole domain, and therefore the liquid saturation, resulting from the capillary curves and the difference between the gas and the liquid pressures, becomes constant in M1 and M2. Let us write the equations satisfied by the asymptotic state at large times:

$$\begin{cases} P_g(\infty) = P_g(0), & \phi^{(1)} S_l^{(1)}(\infty) + \phi^{(2)} S_l^{(2)}(\infty) = \phi^{(1)} S_l^{(1)}(0) + \phi^{(2)} S_l^{(2)}(0) \\ P_c^{(1)}(S_l^{(1)}(\infty)) = P_c^{(2)}(S_l^{(2)}(\infty)), & P_l(\infty) = P_g(\infty) - P_c^{(1)}(S_l^{(1)}(\infty)) = P_g(\infty) - P_c^{(2)}(S_l^{(2)}(\infty)). \end{cases} \tag{26}$$

These equations are satisfied for $P_l(\infty) \simeq -2\ 10^7$ Pa, $S_l^{(1)}(\infty) \simeq 0.844$ and $S_l^{(2)}(\infty) \simeq 0.548$.

Let us finally comment Figure 14, showing the global density of gas. The integral of this quantity with respect to $x$ should remain constant, and equal to the total amount of gas present in the domain. We observe that this property is

graphically respected, in particular at the final time, where the area between the curve in M2 is equal to the difference between the initial and final curves in M1. Figure 14 confirms the lack of displacement of the gas phase in the short times (the curves remain nearly horizontal in domain M1 for $t < 20000$ s ). One can also observe that the penetration of the gas phase into the place previously occupied by the water phase in M2 is mainly driven by the porous medium type equation on the pressure.

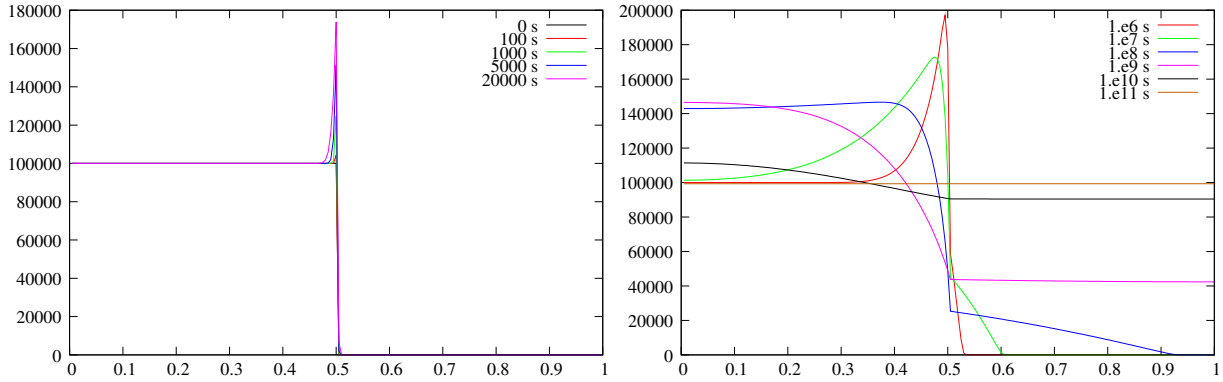


Figure 10: Gas pressure (Pa) with respect to position (m) in Case 1 (no initial gas constituant in M2)

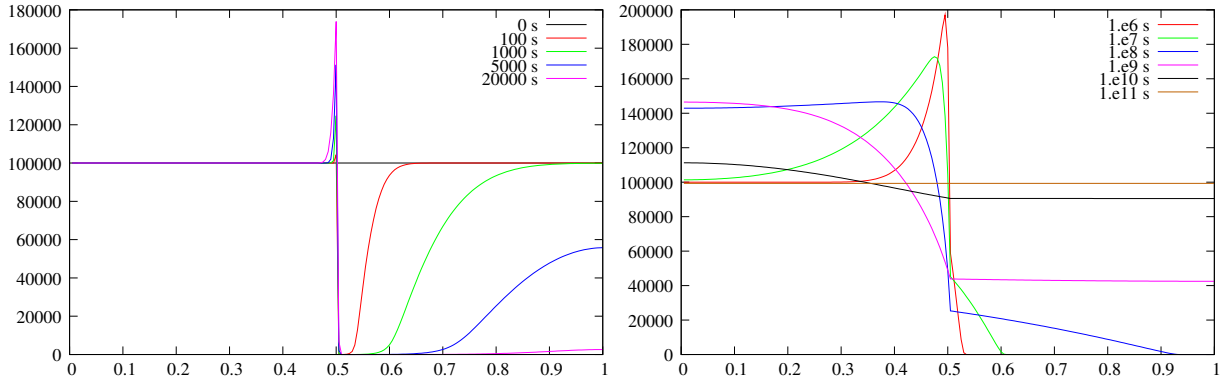


Figure 11: Gas pressure (Pa) with respect to position (m) in Case 2 (water initially saturated with gas in M2).

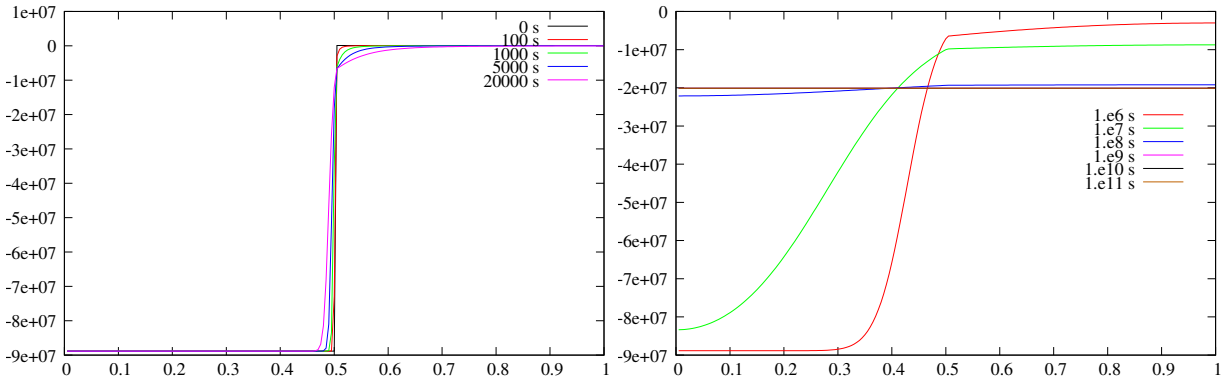


Figure 12: Liquid pressure (Pa) with respect to position (m).

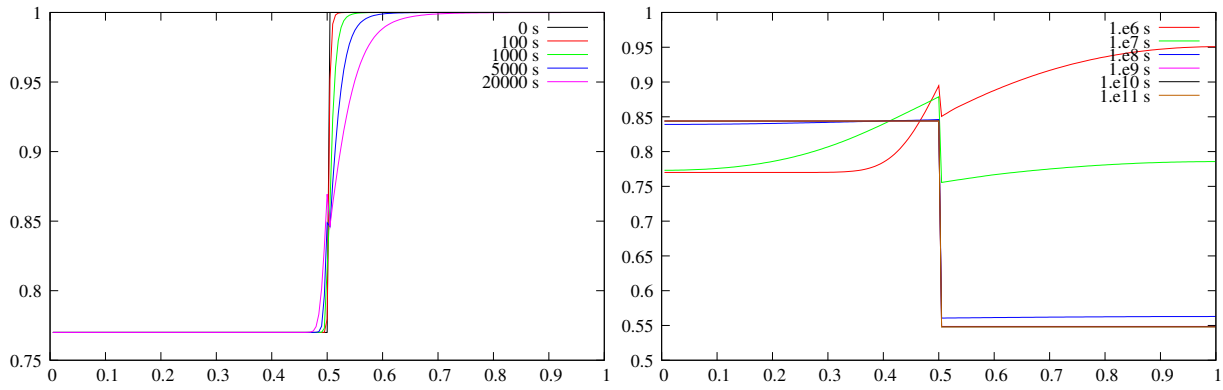


Figure 13: Liquid saturation with respect to position (m).

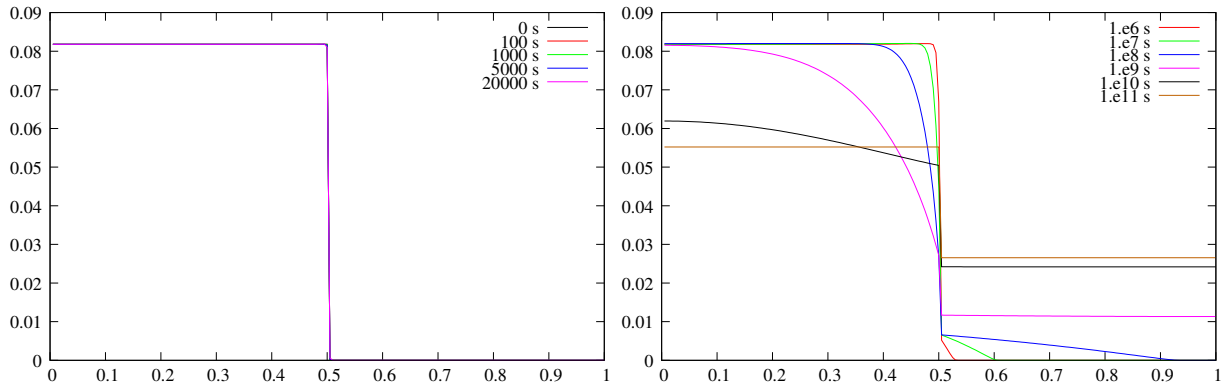


Figure 14: Global density of gas (kg/m$^3$) with respect to position (m).

## 5. Conclusion

The numerical examples show the good behaviour of the formulation introduced in this paper for two-phase flow modelling. Many advantages result from this formulation: it can handle gas injection case, and it can be used for the approximation of immiscible compressible flows. The numerical implementation of this pressure-pressure formulation, thanks to the extension of the SUSHI scheme to this two-phase flow problem, presents stability properties which make this scheme suited for simulations of industrial problems in which the capillary pressure phenomena are dominating (this is the case in the studies concerning nuclear waste storage, but not necessarily the case in oil recovery studies for example).

There now remains to show the properties of the scheme on 3D examples, and on various data with highly contrasted properties.

## Nomenclature

$\mathcal{E}_K$ Set of all faces of control volume $K$

$\mathcal{M}$ Mesh

$\mathbf{F}_p$ Mass flux for phase $p = l, g$

$\mathbf{g}$ Gravity acceleration

$\mathbf{J}_p^c$ Mass diffusive flux for component $c = h, w$ in phase $p$

| | |
|---|---|
| $\mathbf{k}$ | Absolute permeability |
| $C(P)$ | Capacity function |
| $\mu_p$ | Viscosity of phase $p = l, g$ |
| $\mathbf{n}_{K,\sigma}$ | Unit vector normal to $\sigma$ outward to $K$ |
| $\phi$ | Porosity |
| $\rho_p$ | Density of phase $p = l, g$ |
| $\sigma$ | Face of a control volume |
| $\mathbf{x}_\sigma$ | Barycentre of face $\sigma$ |
| $\mathbf{x}_K$ | Centre of control volume $K$ |
| $C_p$ | Molar concentration of phase $p = l, g$ |
| $C_p^c$ | Molar concentration of the component $c = h, w$ in phase $p = l, g$ |
| $D_p^c$ | Diffusion coefficient of component $c = h, w$ in phase $p = l, g$ |
| $d_{K,\sigma}$ | Orthogonal distance between point $\mathbf{x}_K$ and face $\sigma$ |
| $D_{l,K,\sigma}^h$ | Approximation of diffusion flux of component $h$ in phase $l$ outward to $K$ at face $\sigma$ |
| $F_{K,\sigma}$ | Approximation of normal gradient outward to $K$ integrated over face $\sigma$ |
| $F_{p,K,\sigma}^c$ | Approximation of Darcy flux of component $c = h, w$ in phase $p = l, g$ outward to $K$ at face $\sigma$ |
| $g$ | Subscript for gaseous phase |
| $H$ | Henry's law constant at the temperature of the domain |
| $h$ | Superscript for gaseous component |
| $K$ | Control volume, element of $\mathcal{M}$ |
| $K_\sigma$ | Cone with vertex $\mathbf{x}_K$ and basis $\sigma$ |
| $k_{rp}$ | Relative permeability of phase $p = l, g$ |
| $L$ | Control volume, element of $\mathcal{M}$ |
| $l$ | Subscript for liquid phase |
| $m$ | Parameter of Van Genuchten-Mualem law |
| $M^c$ | Molar mass of component $c = h, w$ |
| $m_p^c$ | Volumic mass of component $c = h, w$ in phase $p = l, g$ |
| $n$ | Parameter of Van Genuchten-Mualem law |
| $P_c$ | Capillary pressure |
| $P_p$ | Pressure of phase $p = l, g$ |
| $P_r$ | Parameter of Van Genuchten-Mualem law |
| $R$ | Ideal gas constant |

$S_p$ Saturation of phase $p = l, g$

$S_{gr}$ Parameter of Van Genuchten-Mualem law

$S_{lr}$ Parameter of Van Genuchten-Mualem law

$T$ Temperature

$w$ Superscript for water component

$X_p^c$ Molar fraction of component $c = h, w$ in phase $p = l, g$

## References


[1] A. Abadpour, M. Panfilov, Method of negative saturations for modeling two-phase compositional flow with oversaturated zones, Transp. in Porous Media 79 (2) (2009) 197–214.

[2] O. Angelini, C. Chavant, E. Chénier, R. Eymard, A finite volume scheme for diffusion problems on general meshes applying monotony constraints, SIAM J. Numer. Anal. 47 (6) (2010) 4193–4213.

[3] A. Bourgeat, M. Jurak, F. Smaï, Two-phase, partially miscible flow and transport modeling in porous media; application to gas migration in a nuclear waste repository, Comput. Geosci. 13 (1) (2009) 29–42.

[4] C. Chavant, Cas test diphasique, Tech. rep., Groupement MOMAS (2008).
URL http://sources.univ-lyon1.fr/cas_test/TestBOBG_MOMAS.pdf

[5] C. Chavant, S. Granet, R. Fernandes, Thermo-hydro-mechanical numerical modeling: Application to a geological nuclear waste disposal, in: T. Siegel, R. Luna, T. Hueckel, L. Laloui (eds.), Geotechnical Special Publication No. 157. Part of: Geo-Denver 2007: New Peaks in Geotechnics, Reston, VA: ASCE / Goe Institute, 2007.

[6] O. Coussy, Poromechanics, John Wiley and Sons, Chichester, 2004.

[7] O. Coussy, P. Dangla, R. Eymard, A vanishing diffusion process in unsaturated soils, Int. J. Non-Linear Mechanics 33 (6) (1998) 1027–1037.

[8] EDF, Code_aster (2010).
URL http://www.code-aster.org

[9] R. Eymard, T. Gallouët, R. Herbin, A cell-centered finite-volume approximation for anisotropic diffusion operators on unstructured meshes in any space dimension, IMA J.Numer.Anal. 26 (2) (2006) 326–353.

[10] R. Eymard, T. Gallouët, R. Herbin, A new finite volume scheme for anisotropic diffusion problems on general grids: convergence analysis., C. R., Math., Acad. Sci. Paris 344 (6) (2007) 403–406.

[11] R. Eymard, T. Gallouët, R. Herbin, Discretisation of heterogeneous and anisotropic diffusion problems on general non-conforming meshes. SUSHI: a scheme using stabilisation and hybrid interfaces, to appear in IMA J.Numer.Anal.
URL http://dx.doi.org/10.1093/imanum/drn084

[12] G. Gagneux, M. Madaune-Tort, Analyse mathématique de modèles non linéaires de l'ingénierie pétrolière, vol. 22 of Mathématiques & Applications (Berlin) [Mathematics & Applications], Springer-Verlag, Berlin, 1996, with a preface by Charles-Michel Marle.

[13] P. Gerard, R. Charlier, J.-D. Barnichon, J.-F. Shao, G. Duveau, R. Giot, C. Chavant, F. Collin, Numerical modelling of coupled mechanics and gas transfer around radioactive waste in long-term storage, Journal of Theoretical and Applied Mechanics 38 (1-2) (2008) 25–44.

[14] A. Liakopoulos, Transient flow through unsaturated porous media, Ph.D. thesis, University of California, Berkeley (1965).

[15] M. Mainguy, Modèles de diffusion non-linéaires en milieux poreux. applications à la dissolution et au séchage des matériaux cimentaires, Ph.D. thesis, Thèse de l'École Nationale des Ponts et Chaussées, Paris (1999).

[16] I. Panfilova, Ecoulement diphasiques en milieu poreux : modèle de ménisque, Ph.D. thesis, Institut National Polytechnique de Lorraine (2003).

[17] F. Smaï, Apparition-disparition de phase dans un écoulement diphasique eau/hydrogène en milieu poreux : Injection de gaz dans un milieu saturé en eau pure, Tech. rep., Groupement MOMAS (2009).
URL http://sources.univ-lyon1.fr/cas_test/sature_1.pdf

[18] J. Talandier, Synthèse du benchmark couplex-gaz, Journées scientifiques du GNR MoMaS, Lyon, 4 et 5 septembre 2008.
URL http://momas.univ-lyon1.fr/journees_MoMaS.html

[19] Y.-S. Wua, P. A. Forsyth, On the selection of primary variables in numerical formulation for modeling multiphase flow in porous media, J. Contam. Hydrol. 48 (2001) 277–304.